

# Paramagnetic response of muscle-type systems

M. Caruel<sup>1,\*</sup> and L. Truskinovsky<sup>2</sup>

<sup>1</sup>*MSME, CNRS- UMR 8208, 61 Avenue du Général de Gaulle, 94010 Créteil, France*

<sup>2</sup>*LMS, CNRS-UMR 7649, Ecole Polytechnique, 91128 Palaiseau Cedex, France*

(Dated: May 11, 2022)

We provide a prototypical description of mechanically-induced collective conformational change (folding), relevant in a variety of biological contexts from muscle contraction to hair cell gating and integrin binding. Our study is inspired by the seminal Huxley-Simmons (HS) model which we reinterpret from the perspective of stochastic dynamics involving rigidly coupled bi-stable elements. In this interpretation the HS model can be mapped to a paramagnetic Ising model, however, the equivalence is not complete due to the presence of elastic elements responsible for negative susceptibility and quasi-critical behavior. We go beyond the conventional chemo-mechanical description of such systems, revealing both its strengths and its limitations.

## I. INTRODUCTION

The short time mechanical response of skeletal muscles is nontrivial, for instance, if a tetanized muscle is suddenly shortened, it tightens up. A series of mechanical experiments involving rapid shortening were conducted in [1–5] with the goal of distinguishing passive from active contributions to tension recovery. It was shown that the first phase of the response is quasi elastic during which the tension drops almost instantaneously. During the second phase, tension recovers to a level which depends nonlinearly on the amplitude of the shortening. This fast force recovery, lasting about 1 ms, precedes a considerably slower phase at the end of which the tension fully returns to its original value. Such more sluggish recovery, taking place on a 100 ms time scale, is usually interpreted as an active process driven by ATP hydrolysis [6, 7]. In contradistinction, the process of fast force recovery is usually interpreted as passive.

The phenomenon of passive fast force recovery was first modeled theoretically in the pioneering work of A.F. Huxley and R.M. Simmons [5]. It was attributed to a rapid conformational change (folding) in an assembly of elastically coupled myosin cross-bridges. The idea of bi-stability in the structure of myosin heads, giving rise to such power-stroke, is supported by crystallographic studies [8, 9] and the whole scenario is in agreement with the fact that the power-stroke is the fastest step in the main acto-myosin autocatalytic cycle [10, 11].

Behind the passive folding of cross-bridge heads is a thermally induced random walk in a complex multi-dimensional energy landscape biased by mechanical loading [12–14]. Under the assumption that the system behaves cooperatively, such random work can be projected on a low dimensional energy landscape. The construction of this landscape implies equilibrium relaxation of the other degrees of freedom and when the energy barriers associated with this landscape are high comparing

to thermal fluctuations, the remaining stochastic dynamics can be modeled within the Kramers approximation. This approach, reducing the dynamics to a set of chemical reactions, was adopted without formal justification by Huxley and Simmons (HS) who replaced the two conformations of a myosin head by two discrete chemical states and modeled the fast force recovery in length clamp conditions (hard device), as a jump process. The information about the energetic biases between the states (and the corresponding energy barriers) was encoded into the prescribed reaction rates. The price of switching from mechanics to chemistry was that reaction constants became poorly constrained functions of the “mechanical configuration” of the system.

The ensuing quasi-chemical model was later generalized by Hill [15, 16] and refined in the muscle context through the inclusion of numerous additional chemical states with kinetics prescribed by a set of phenomenologically defined functions [7, 17–19]. Similar descriptions of mechanically driven conformational changes have almost immediately reappeared in the study cell adhesion [13, 20] and in the context of hair cell gating [21, 22]. Other closely related phenomena include mechanical denaturation of RNA and DNA hairpins [23–25], unzipping of biological macromolecules [26–32], collective action of SNARE proteins during opening of synaptic pores [33] and even formation of ripples in graphene sheets [34]. For all these systems the quasi-chemical HS model can be viewed as a mean-field prototype.

The goal of the present paper is to go beyond the chemo-mechanical description and to re-formulate the original HS model in the abstract language of statistical mechanics. Such changing of the focus allows one to find the domain of validity of the implied dimension reduction and address the features observed in various applications of this model from the common perspective of stochastic dynamics of coupled bi-stable elements [35–38]. In such interpretation the HS model becomes equivalent to the paramagnetic Ising model whose thermodynamic and kinetic properties are well known [39]. The equivalence, however, is not complete because of the presence of an elastic element which is responsible for the

---

\* matthieu.caruel@u-pec.fr

meta-material behavior and some critical features of the resulting model.

We build on the results of [40] and [41] where this approach was first executed for a soft-spin analog of the HS system. The hard-spin system, equivalent to the original HS model, was studied at zero temperature in [42]. In the present paper we extend the analysis of the hard-spin system to finite temperatures which allows a direct comparison of the HS statistical model with its chemo-mechanical analogs. In contrast to the standard chemo-mechanical descriptions our model accounts for thermal behavior, fluctuations and finite size effects. Given that our analysis encompasses the chemo-mechanical approximation of HS, we can reveal both its strengths and its limitations.

The analytical transparency of our stochastic model, allowing one to explicitly compute the free energy function, is due to the fact that individual bi-stable elements, linked through a rigid backbone, do not interact. They interact only with an external field imposed by a hard loading device (prescribed displacement) which makes the mean-field approximation exact. It is then sufficient to deal with a single element and even in the absence of correlations, the phase space becomes one dimensional making the mapping on a chemical reaction viable. The mean-field nature of the system ensures that the dependence of the marginal free energy on the reaction coordinate is bi-stable which opens the possibility for describing kinetics in terms of the Kramers approximation [43] and ultimately justifies the HS approach.

In this situation, our main result, *vis-à-vis* the chemo-mechanical approximation, focusing exclusively on averages, is the account for fluctuations. We make an important observation that the physiologically most relevant state is the state where the variance of the fluctuations is the largest. While the “critical” features of the corresponding point in the parameter space, characterized by the zero stiffness, have nothing to do with cooperative behavior, the ensuing phenomenology is reminiscent of the near critical behavior in Ising system with controlled magnetization or liquid-vapor system with controlled volume. Our analysis also reveals that in the length clamp condition the folding process described by HS model is highly de-synchronized which contradicts the usual intuitive interpretation of the quick force recovery as resulting from cooperative power-stroke. This observation suggests that the original HS model misses a crucial coupling between individual folding elements that can give rise to cooperative folding [41].

To build additional bridges between the theory and observations, we show that the effective stiffness of the HS system can be represented as a sum of an enthalpic term proportional to the number of bi-stable elements and an entropic term which characterizes the contribution due to fluctuations. This analytical result may be readily verified experimentally since both fluctuations and total stiffness are measurable quantities. Our analysis also suggests that the response of a bundle with finite number of

bi-stable units must exhibit a series of jumps that should be detectable in experiments under length clamp conditions. Another potentially verifiable prediction of our model concerns the anomalous behavior of the specific heat and the difference between adiabatic and isothermal responses.

In addition to studying equilibrium, we following [44] develop a kinetic equation for the describing the dynamics of the folding-unfolding processes in an isothermal HS system with finite number of elements. We compare the predicted evolution with the direct numerical study of stochastic dynamics and recover the results of the chemo-mechanical model from the analysis of the evolution of the first moments.

The paper is organized as follows. In Section II we deal with a single folding element and show that in this way all the results obtained by Huxley and Simmons can be fully recovered. In Section III we extend the analysis to a system comprised of  $N$  such elements connected in parallel. We compute the marginal free energy characterizing the internal configuration of the system and study the structure of the fluctuations. Our Section IV contains the analysis of the kinetics for a single bi-stable element and for the parallel bundle of such elements. In the last Section V we summarize our results and mention some open problems.

## II. SINGLE HS ELEMENT

The original Huxley-Simmons model [5] deals essentially with a *single* folding element (cross-bridge) and in this Section we study the statistical mechanics of the corresponding mechanical system with one degree of freedom.

### A. The mechanical model

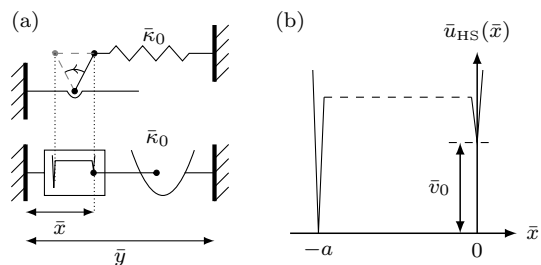


FIG. 1. Huxley-Simmons (HS) model of a single cross-bridge: (a) mechanical representation a myosin head; (b) energy landscape representing two chemical states. The conformation is characterized by the spin variable  $\bar{x}$ . The bistable element is linked in series with a linear spring of stiffness  $\bar{\kappa}_0$ .

The HS element can be viewed as an elastic spring with stiffness  $\bar{\kappa}_0$  (denoted by  $K$  in [5]) that is connected

in series with a bi-stable spin unit, see Fig. 1. The two spin states represent the two conformations of the myosin head and the spin variable  $\bar{x}$  (denoted by  $-\theta$  in [5]) takes the values 0 (pre-power-stroke or unfolded conformation) and  $-a$  (post-power-stroke or folded conformation). The total length  $\bar{y}$  will be our control parameter and the main quantity of interest will be the developed tension  $\bar{\sigma} = \bar{\kappa}_0(\bar{y} - \bar{x})$ .

We choose  $a$ , denoted by  $h$  in [5], as the “reference” size of the conformational change equal to the distance between two infinitely localized energy wells and we denote by  $\bar{v}_0$  the intrinsic energy bias distinguishing the two states; see Fig. 1(b). The energy of the spin element can be now written as

$$\bar{v}_{\text{HS}}(\bar{x}) = \begin{cases} \bar{v}_0 & \text{if } \bar{x} = 0, \\ 0 & \text{if } \bar{x} = -a, \\ \infty & \text{otherwise.} \end{cases} \quad (1)$$

The energy  $\bar{v}_0$  is an implicit representation of the ATP-fueled activity. It will be clear in what follows that the presence of such bias (mimicking tetanization) ensures that in the reference state the series spring is stretched.

It will be convenient to use dimensionless variables and if we choose  $a$  as our characteristic distance, the non-dimensional spin variable  $x = \bar{x}/a$  will take values 0 or  $-1$ . It is then natural to normalize the total energy of the system by  $\bar{\kappa}_0 a^2$  and write it in the form

$$v(x; y) = \bar{v}/(\bar{\kappa}_0 a^2) = (1+x)v_0 + \frac{1}{2}(y-x)^2, \quad x = \{0, -1\}, \quad (2)$$

where  $y = \bar{y}/a$  is the length of the element that includes the bi-stable unit and a linear spring and  $v_0 = \bar{v}_0/(\bar{\kappa}_0 a^2)$ . For  $y > y_0$  (resp.  $y < y_0$ ), where  $y_0 = v_0 - 1/2$ , the global minimum of this energy corresponds to the pre-power-stroke state (resp. post-power-stroke state); in [5], the shifted elongation  $y - y_0$  was denoted by  $y$ .

Notice that our variable  $y$  plays a role of the external (magnetic) field for the spin variable  $x$  and therefore our model resembles the zero dimensional Ising model of paramagnetism [39]. However, due to the presence of the linear spring this Ising model is unusual: the external field has its own “energy” represented by the quadratic term in  $y$ . In the HS experiments a muscle was loaded in a hard device known also as length clamp. This means that the total length of the system  $y$  should be the control parameter which makes this term seemingly irrelevant. Later we show that this is not the case and that the energy of the “external field”, bringing additional stiffness into the system, is responsible for several interesting mechanical effects.

## B. Thermodynamic equilibrium

Denoting by  $T$  the absolute temperature we can write the equilibrium probability density for the configuration

of a single element  $x$  at fixed  $y$  in the form

$$\rho_1(x; y, \beta) = \frac{1}{Z_1(y, \beta)} \exp[-\beta v(x; y)], \quad (3)$$

where  $\beta = \kappa a^2/(k_b T)$  is the inverse dimensionless temperature,  $k_b$  is the Boltzmann constant and  $v$  is the energy (2). The partition function for a single element is then

$$Z_1(y, \beta) = \exp\left[-\frac{\beta}{2}(y+1)^2\right] + \exp\left[-\beta\left(\frac{y^2}{2} + v_0\right)\right]. \quad (4)$$

From (3) we can compute the average conformation of the crosslinker namely,

$$\begin{aligned} \langle x \rangle(y, \beta) &= \sum_{x=\{0,1\}} x \rho_1(x; y, \beta) \\ &= -\frac{1}{2} \left\{ 1 - \tanh\left[\frac{\beta}{2}(y - y_0)\right] \right\}, \end{aligned} \quad (5)$$

– the analog of Eq. (15) in [5] where the corresponding variable was denoted by  $n_2$ . In paramagnetic interpretation  $\langle x \rangle(y, \beta)$  is the analog of the “average magnetization”, the parameter conjugate to the “applied magnetic field”  $y$ .

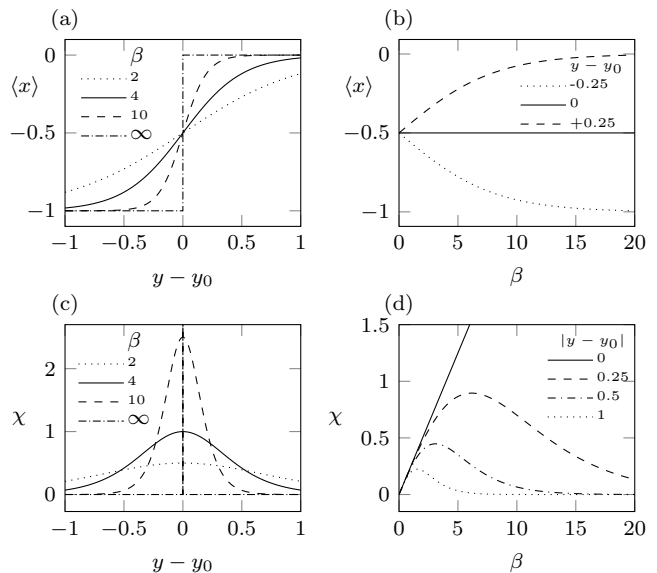


FIG. 2. Average conformation and susceptibility of a single HS element in thermal equilibrium. (a), average configuration as function of the applied elongation at different temperatures; (b), average configuration as function of temperature at different elongations; (c), susceptibility as function of elongation at different temperatures. (d), susceptibility as function of the temperature for selected values of  $y$ . Here we have  $v_0 = 1$  implying  $y_0 = 1/2$ .

The dependence of  $\langle x \rangle$  on the relative elongation  $y - y_0$  is illustrated in Fig. 2(a). In the zero temperature limit the system driven through  $y$ , follows the global minimum

of the internal energy (2) and the population of the wells changes discontinuously at  $y = y_0$  [42]. As the temperature increases, the transition smoothens and in the limit  $\beta \rightarrow 0$  we have  $\langle x \rangle = 1/2$  independently of the elongation as illustrated in Fig. 2(b).

By differentiating Eq. 5 with respect to  $y$  we obtain the explicit representation of the equilibrium susceptibility

$$\chi(y, \beta) = \frac{\partial}{\partial y} \langle x \rangle (y, \beta) = \beta \langle [x - \langle x \rangle (y, \beta)]^2 \rangle \quad (6)$$

that is always positive as expected in paramagnetic systems. We emphasize that it is proportional to the variance of  $x$

$$\langle [x - \langle x \rangle (y, \beta)]^2 \rangle = (1/4) \operatorname{sech}[\beta(y - y_0)/2]^2, \quad (7)$$

used in what follows as a measure of the intensity of fluctuations.

In the zero temperature limit the variance of  $x$  is negligible at large absolute elongations. Instead, at  $y = y_0$ , the strength of fluctuations is independent of temperature and we obtain that  $\chi = \beta/4$ , which is an analog of the Curie law in paramagnetism [39], see Fig. 2 (c,d). The point  $y = y_0$  is associated with the physiological state of isometric contractions, and there is indeed considerable experimental evidence that fluctuations are large in this particular state [45–48]. For other values of elongation  $y \neq y_0$  one can define a characteristic temperature  $\beta = \beta_\chi^*(y)$  solving the equation

$$\beta_\chi^*(y - y_0) \tanh \left[ \frac{\beta_\chi^*}{2} (y - y_0) \right] = 1.$$

In this point fluctuations are maximized, see Fig. 2 (d). For temperatures smaller than the characteristic temperature the system is essentially “frozen” and therefore resistant to fluctuations and the same is true for large temperatures where the system is maximally disordered [39].

In the context of skeletal muscles, the obtained results may already serve as a guidance for new experiments. For instance, detecting the state of maximum susceptibility one can identify it with the configuration where  $\langle p \rangle = 1/2$  and this conclusion can be tested independently by X-ray diffraction techniques [49]. Moreover, by measuring the fluctuations of cross bridge configurations one can search for potential deviations from the static fluctuation-dissipation relation (6) implying the presence of out-of-equilibrium active processes behind the power-stroke, as it was advocated in [50].

### C. Mechanical behavior

The non-dimensional free energy of a single HS element in a hard device can be computed explicitly,

$$f(y, \beta) = -\frac{1}{\beta} \log [Z_1(y, \beta)] = \frac{1}{2}y^2 + v_0 + \frac{y - y_0}{2} - \frac{1}{\beta} \ln \left\{ 2 \cosh \left[ \frac{\beta}{2} (y - y_0) \right] \right\}. \quad (8)$$

Its dependence on elongation is illustrated in Fig. 3(a). We observe that for  $\beta \leq 4$  (large temperatures) the free energy is convex while for  $\beta > 4$  (small temperatures) it is non-convex. The emergence of the “critical temperature”  $\beta = \beta_c = 4$  is a feature of ferromagnetic rather than paramagnetic systems and in our case it results from the presence of an additional quadratic energy associated with the “applied field”  $y$ .

To study the mechanical manifestations of the implied “criticality” we introduce the tension  $\sigma = \bar{\sigma}/(\kappa_0 a) = y - x$  experienced by the series linear spring. Due to the presence of the quadratic term  $y^2$  in the energy, the conjugate variable to elongation  $y$  is not the average “magnetisation”  $\langle x \rangle$  but the average tension  $\langle \sigma \rangle$  which is a linear function of  $\langle x \rangle$ . The convexity properties of the free energy can be then illustrated through the averaged tension-elongation relation  $\langle \sigma \rangle (y, \beta) = \partial f(y, \beta)/\partial y$ . We obtain

$$\langle \sigma \rangle (y, \beta) = v_0 + y - y_0 - \frac{1}{2} \tanh \left[ \frac{\beta}{2} (y - y_0) \right] \quad (9)$$

which corresponds to Eq. 16 in [5]. The (active) tension generated in the reference state  $y = y_0$  where the bottoms of the two energy wells in (2) are at the same level, is  $\sigma_0 = \langle \sigma \rangle (y_0) = v_0$ . This state represents *isometric tetanus* controlled in the HS theory by the energy bias  $v_0$ .

The dependence of  $\langle \sigma \rangle$  on  $y$  is shown in Fig. 3(b) for different values of temperature. We observe that while the relation  $\langle x \rangle (y)$  at fixed temperature is always monotone, as it is supposed to be in a classical paramagnetic spin system, see Fig. 1, the dependence of the tension  $\langle \sigma \rangle$  on its conjugate variable  $y$  can be non-monotone, see Fig. 3(b). Behind the non-monotonicity is the fact that the equilibrium stiffness

$$\begin{aligned} \kappa(y, \beta) &= \frac{\partial}{\partial y} \langle \sigma \rangle (y, \beta) = 1 - \chi(y, \beta) \\ &= 1 - \beta \langle [\sigma - \langle \sigma \rangle (y, \beta)]^2 \rangle \end{aligned} \quad (10)$$

is a sign indefinite sum of two terms. The first constant term is the (normalized) enthalpic stiffness of the series spring. The second term proportional to the variance of tension contains the entropic contribution; it vanishes for  $|y - y_0| \gg 1$  where the system is linear and dominates around  $y = y_0$  where, at  $\beta = \beta_c$  the tension-elongation relation develops a zero stiffness “critical” state. Interestingly, Huxley and Simmons selected exactly this value

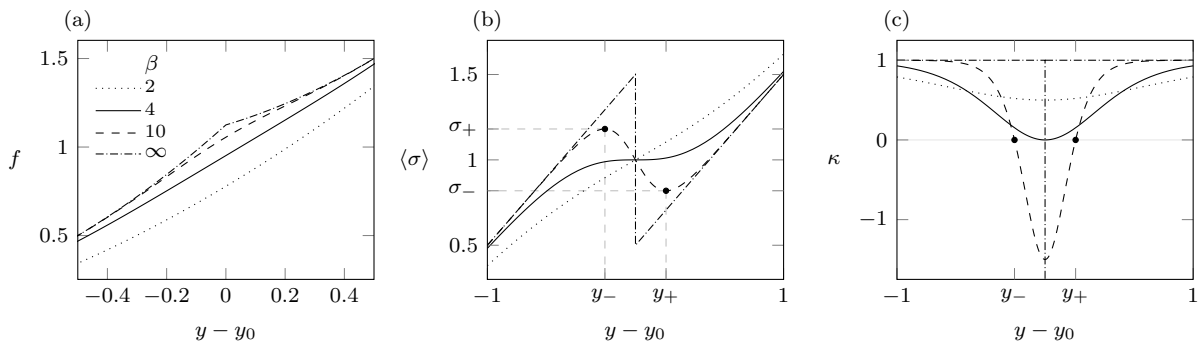


FIG. 3. Thermal equilibrium properties of the HS model in a hard device for different values of temperature. (a) Helmholtz free energy; (b) tension-elongation relations; (c) stiffness. Parameters are,  $v_0 = 1$ , ensuring that  $\sigma_0 = 1$ ,  $y_0 = v_0 - 1/2 = 1/2$ ;  $\beta = 2$  (dotted),  $\beta = 4$  (solid),  $\beta = 10$  (dashed) and  $\beta \rightarrow \infty$  (dash-dotted). In the limit  $\beta \rightarrow \infty$ , corresponding to zero temperature, the stiffness  $\kappa$  diverges at  $y = y_0$ , see (d).

$\beta_c = 4$  (which is  $4/\alpha = 8$  nm in the units adopted in [5]) to reproduce their experiments. However, the “criticality” in HS system placed in a hard device is fictitious as in van-der-Waals gas under controlled volume. The situation is therefore different from the behavior of a ferromagnetic system with field control where zero susceptibility signals the presence of a real critical point.

The interplay between enthalpic and entropic contributions to stiffness is most transparent at  $y = y_0$  where  $\kappa = 1 - \beta/4$  which can be viewed as an adaptation of the Curie law for our system. The negative stiffness, which is a result of non-additivity of this system, prevails at subcritical temperatures. It suggests that shortening of the element should result in a tension increase which can be interpreted as a meta-material behavior [41, 51]. At supercritical temperatures the stiffness becomes positive eventually reaching the enthalpic value  $\kappa = 1$ . A detail study of the domain of negative stiffness (spinodal region) in the space of parameters  $\beta, y$  is presented in Appendix A.

Finally we remark that since

$$\langle \sigma \rangle (y, \beta) = y - \langle x \rangle (y, \beta),$$

and

$$\left\langle [\sigma - \langle \sigma \rangle (y, \beta)]^2 \right\rangle = \left\langle [x - \langle x \rangle (y, \beta)]^2 \right\rangle, \quad (11)$$

the fluctuations of tension are the direct consequence of the fluctuations of the conformation and therefore the study of the “noisy” traces for the force generated by a muscle can be used as an experimental window into the microscopic configuration of the system.

#### D. Thermal behavior

While the prevailing types of experiments on skeletal muscles have been focused on the mechanical behavior [52–59], the study of their thermal/calorimetric response can be as informative [60–64]. Here as in the case of

mechanical behavior, the HS model provides all the necessary information. For instance, the entropy of the HS element can be also computed explicitly

$$\begin{aligned} s(y, \beta) &= -\beta \frac{\partial}{\partial \beta} \log [Z_1(y, \beta)] + \log [Z_1(y, \beta)] \\ &= \log \left\{ 2 \cosh \left[ \frac{\beta}{2} (y - y_0) \right] \right\} \\ &\quad - \frac{\beta}{2} (y - y_0) \tanh \left[ \frac{\beta}{2} (y - y_0) \right], \end{aligned} \quad (12)$$

The behavior of the function  $s(y, \beta)$  is illustrated in Fig. 4(a,c) where we see that the degree of disorder is maximal in the state of isometric contractions. Notice that the entropy depends on a single normalized coordinate  $\beta (y - y_0)$  combining both control parameters, temperature and displacement. Therefore for  $y > y_0$ , an isoentropic shortening would lead to an increase in  $\beta$  and thus to a decrease of temperature. Similar effect in a paramagnetic spin system is known as cooling by adiabatic demagnetization. In HS system the applied field  $y - y_0$  can be both positive and negative and in the case,  $y < y_0$  a shortening would lead to a temperature increase which can be in principle measured in experiment.

The expression for entropy (12) can be also rewritten in the form  $s = \beta \langle v \rangle - \beta f$  where  $\langle v \rangle$  is the average internal energy

$$\begin{aligned} \langle v \rangle (y, \beta) &= -\frac{\partial}{\partial \beta} \log [Z(y, \beta)] \\ &= \frac{y^2}{2} + v_0 - (y - y_0) \langle x \rangle (y, \beta) \end{aligned} \quad (13)$$

In contrast to the equilibrium free energy, which decreases with temperature while acquiring convexity, the average internal energy increases with the same effect. In the zero temperature (athermal) limit  $\beta \rightarrow \infty$  the average internal energy converges to the global minimum of the elastic energy while becoming non-convex, see Appendix B for more detail.

The variance of the internal energy

$$\langle [v - \langle v \rangle (y, \beta)]^2 \rangle = (y - y_0)^2 \langle [x - \langle x \rangle (y, \beta)]^2 \rangle. \quad (14)$$

is known to be a measure of the specific heat [39]

$$\begin{aligned} c(y, \beta) &= -\beta \frac{\partial}{\partial \beta} s(y, \beta) = -\beta^2 \frac{\partial}{\partial \beta} \langle v \rangle (y, \beta) \\ &= \beta^2 \langle [v - \langle v \rangle (y, \beta)]^2 \rangle. \end{aligned} \quad (15)$$

It bears the same form as in paramagnetic spin systems

$$c(y, \beta) = \left\{ \frac{\beta}{2} (y - y_0) \operatorname{sech} \left[ \frac{\beta}{2} (y - y_0) \right] \right\}^2, \quad (16)$$

similarly depending only on the combination  $\beta(y - y_0)$ .

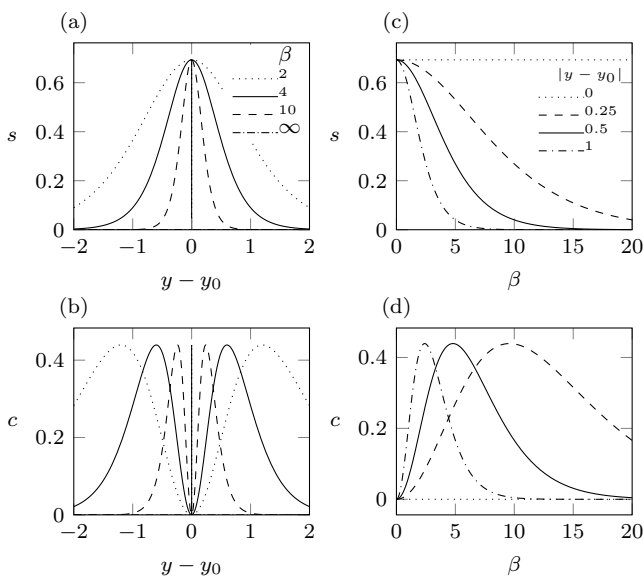


FIG. 4. Entropy and specific heat in thermal equilibrium. (a,b) Entropy  $s$  and specific heat  $c$  as function of the elongation for  $\beta = 2$  (dotted),  $\beta = 4$  (solid),  $\beta = 10$  (dashed) and  $\beta \rightarrow \infty$  (dash-dotted). (c,d) Entropy  $s$  and specific heat  $c$  as function of the temperature for  $y = y_0 \pm 0$  (dotted), 0.25 (dashed), 0.5 (solid) and 1 (dot-dashed). Here  $v_0 = 1$ .

We observe that since at  $y = y_0$ , the entropy is temperature insensitive ( $s(y_0) = \log(2)$ ), the specific heat vanishes. Similarly at large elongations, the systems gets more and more ordered and temperature changes no longer affect the entropy. As a result the specific heat is maximized at another characteristic value of the temperature  $\beta = \beta_c^*$  solving the equation

$$\beta_c^* (y - y_0) \tanh \left[ \frac{\beta_c^*}{2} (y - y_0) \right] = 2.$$

The fact that the specific heat vanishes in the physiological state of isometric contractions (at  $y = y_0$ ) makes this configuration robust with respect to temperature

changes which is obviously advantageous. The low value of the specific heat suggests that in this state the system has only few effective degrees of freedom and works like a mechanism. This state is well localized since already small deviation from the point  $y = y_0$  results in a considerable growth of specific heat making the system much less predictable. To verify these results in the case of skeletal muscles it is of interest to conduct experiments where rapid temperature increments are applied to a tetanized muscle myofibril while the released heat is recorded by calorimetric methods [52, 60–65].

The knowledge of the thermal properties of the HS element allows one to address the question whether the isothermal approximation, universally accepted inside the quasi-chemical approach, is justified when applied to fast force recovery experiments. For instance, the assumption that temperature remains constant in such experiments can be challenged by the observation that heat removal/delivery may be rate limiting. In this situation, the assumption of an adiabatic response to sufficiently fast solicitation would be more appropriate and below we explore the consequences of this premise.

To remain within the thermodynamic framework, we replace the task of computing the actual adiabats by computing the isoentropes that we'll be still referring to as adiabats. As the entropy of the system depends solely on  $\beta|y - y_0|$ , see Eq. 12, the temperature varies along such adiabats proportionally to the elongation. In Fig. 5(a) we show the temperature changes along adiabats parametrized by the values of the entropy which is kept constant. Notice that at  $y = y_0$  the inverse temperature  $\beta$  along an adiabat diverges, which means that reaching the state of isometric contractions adiabatically brings about infinite cooling. It would be of interest to test this prediction in a targeted experiment where the system is first equilibrated after shortening (the  $T_2$  state of HS [5]) and then stretched to reach again the state of isometric contractions (the  $T_0$  state of HS [5]). Instead, if the initial state is  $y = y_0$  corresponding to the maximum entropy, even small adiabatic length change would lead to a dramatic increase of temperature ( $\beta \rightarrow 0$ ). It is also of interest that for  $y > y_0$  shortening leads to cooling while for  $y < y_0$  it leads to heating.

The adiabatic response of the micro-configuration of the system to abrupt “length steps” is illustrated in Fig. 5 (b). According to Eq. 5 for the adiabat passing through the point  $y = y_0$  the average configuration remains frozen at  $\langle x \rangle = -1/2$ ; the behavior of micro-configuration along the isotherm passing through the same point is very different as we show in Fig. 5 (b) by drawing an isotherm corresponding to  $\beta = 10$ . Since equilibrium tension along the adiabats depends linearly on  $\langle x \rangle$ , the adiabatic stress response to shortening from  $y = y_0$  is quasi-linear-elastic even though the temperature undergoes considerable growth. One can then conjecture that the “instantaneous” elastic phase of the mechanical response of skeletal muscles to abrupt shortening ( $T_1$  of HS [5]) is a manifestation of the adiabatic phase of the relaxation and

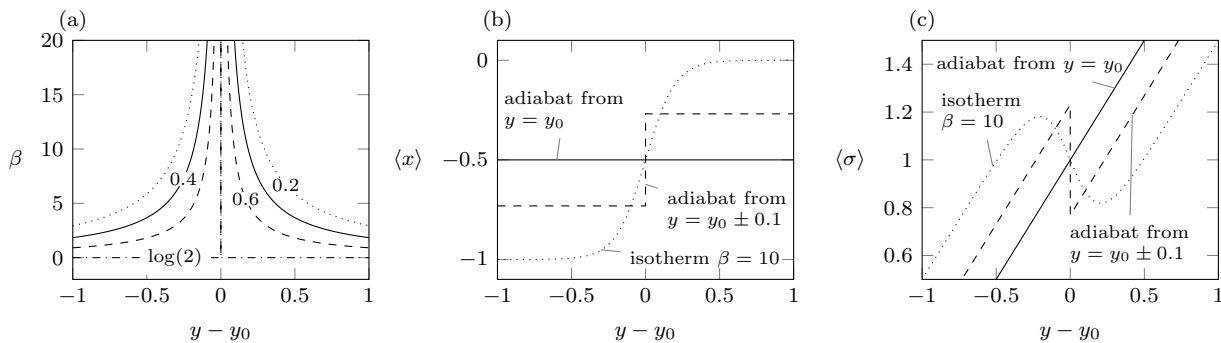


FIG. 5. Adiabatic response. (a) evolution of temperature as function of the applied loading along adiabats for  $s = 0.2$  (dotted),  $s = 0.4$  (solid) and  $s = 0.6$  (dashed). (b) Average conformation following adiabatic length change from two different thermal equilibrium initial conditions  $y = y_0$  (solid) and from  $y = y_0 \pm 0.1$  (dashed) at  $\beta = 10$ . The isothermal response is represented by the dotted line. (d) adiabatic tension-elongation relations. Dotted line, isotherm response for  $\beta = 10$ ; dashed line, adiabatic response with initial state at  $y - y_0 = \pm 0.1$  with  $\beta = 10$ ; solid line, adiabatic response with initial state at  $y = y_0$  with  $\beta = 10$ . The dotted line shows the corresponding isotherm. Here  $v_0 = 1$ .

interpret the subsequent fast force recovery to the equilibrium value ( $T_2$  of HS [5]) as a slower isothermal relaxation to equilibrium. A significant transient temperature increase during the instantaneous phase of unloading is potentially measurable in experiments that could then serve as an ultimate test of such non-isothermal theory. For instance, if the fiber shortens from an eccentric state through the state  $y = y_0$ , the temperature variation will be non-monotone which should experimentally verifiable.

For the adiabats starting at  $y \neq y_0$  Eq. 5 states that the average configuration  $\langle x \rangle$  remains frozen at its initial value till the loading reaches the point  $y = y_0$ . At this point the condition of continuity of entropy requires that the configuration changes discontinuously. Indeed, because of adiabatic cooling at  $y - y_0$  the temperature here goes to zero and the response becomes discontinuous. More specifically, along an adiabat starting at  $y = y_{\text{in}}$  with temperature  $\beta = \beta_{\text{in}}$  we have

$$\beta_{\text{ad}} = \beta_{\text{in}} \frac{|y_{\text{in}} - y_0|}{|y - y_0|}.$$

Then the average configuration evolves according to

$$\langle x \rangle_{\text{ad}}(y, \beta) = -\frac{1}{2} + \frac{1}{2} \tanh \left[ \frac{\beta_{\text{in}} |y_{\text{in}} - y_0|}{2} \text{sign}(y - y_0) \right] \quad (17)$$

and the presence of a jump at  $y = y_0$  becomes obvious. The resulting scenario is illustrated in Fig. 5(b) for the case where the initial state is  $y = y_0 \pm 0.1$ . It is in stark contrast with continuous evolution of the configuration along a typical isotherm also shown for comparison in Fig. 5(b, dotted line). The corresponding adiabatic tension-elongation relations are then piece-wise linear with stiffness equal to one for all  $y \neq y_0$  and a finite jump at  $y = y_0$ , see Fig. 5(c). The presence of a discontinuity suggests the possibility of non-monotone, meta-material type variation of tension during “instantaneous elastic” response interpreted as adiabatic deformation.

The associated temperature variations should be also detectable. For instance, a stretch originated at  $y = y_0 - 0.1$  would lead first to a linear tension increase accompanied with a temperature decrease and then to a sudden tension drop at zero temperature followed by a new linear increase of tension accompanied now by a temperature growth.

### III. PARALLEL BUNDLE OF HS ELEMENTS

The analysis of the original HS element presented in Section II shows that the equilibrium behavior of the system can be fully recovered by applying the classical tools of statistical mechanics. However, a priori, this approach does not provide information about the behavior of a system comprised of many HS elements. In particular, we still do not know whether different cross-bridges in skeletal muscles acts cooperatively. In this Section we study this question by using the assumption that different HS elements are connected in parallel through a rigid backbone. This was an implicit assumption in the original theory of Huxley and Simmons and we show that it makes the consideration of a single HS element fully sufficient to answer the questions about the collective behavior of  $N$  HS elements.

#### A. The mechanical model

To access the degree of cooperativity among the HS elements coupled through a common backbone, see Fig. 6(a), we now consider  $N$  such elements attached in parallel between two rigid planes, see Fig. 6(b). The energy of this bundle can be written as

$$e(\mathbf{x}; y) = \frac{1}{N} \sum_{i=1}^N \left[ (1 + x_i) v_0 + \frac{1}{2} (y - x_i)^2 \right], \quad (18)$$

where  $\mathbf{x} = \{x_1, \dots, x_N\}$ . One can see that the individual bi-stable elements in this system do not interact between themselves while they all interact with the same external field  $y$  that is due to hard device constraint is not affected by the micro-configuration of the system. In the language of magnetism this is a one dimensional paramagnetic system. For such systems the dimensionality is in fact irrelevant because all elements behave identically. While this excludes cooperativity, we can expect all the results obtained for the zero dimensional model to remain valid.

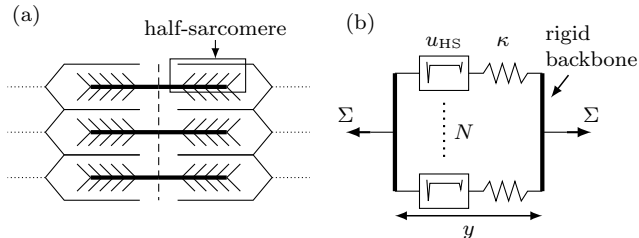


FIG. 6. Schematic representation of acto-myosin filaments organisation in a superstructure of half-sarcomeres (a). (b) A single half-sarcomere represented as a cluster containing  $N$  cross-linkers, see Fig. 1. The control parameter is the total elongation  $y$  and the total tension generated by the system is denoted by  $\Sigma$ .

## B. Thermodynamic equilibrium

In thermal equilibrium, the probability density for a micro-state  $\mathbf{x}$  with  $N$  elements reads

$$\rho(\mathbf{x}; y, \beta) = Z(y, \beta)^{-1} \exp[-\beta e(\mathbf{x}; y)] \quad (19)$$

where the partition function is

$$Z(y, \beta) = \sum_{\mathbf{x} \in \{0, -1\}^N} \exp[-\beta N e(\mathbf{x}; y)] \quad (20)$$

Due to the additivity of the energy (reflecting the parallel connection of the elements) we obtain  $Z(y, \beta) = [Z_1(y, \beta)]^N$ , where  $Z_1$  is given by (4). Therefore  $\rho(\mathbf{x}; y, \beta) = \prod_{i=1}^N \rho_1(x_i; y, \beta)$  and the total free energy can be written as

$$F(y, \beta) = N f(y, \beta),$$

where the expression for the free energy of a single HS element  $f$  is given by (8); this formula is analogous to the corresponding result for paramagnetic Ising model and other mean-field type systems, e.g. [27]. Similarly, all extensive equilibrium properties in this mean-field system will also behave additively and in what follows all extensive parameters will be normalized by  $N$ .

To shed light on the internal configuration of the system we introduce the fraction of HS elements in the

folded (post-power-stroke) conformation

$$p = -\frac{1}{N} \sum_{i=1}^N x_i,$$

which plays in our case the role of the order parameter. The internal energy (per cross-linker) of the system corresponding to a given  $p$  can be written as,

$$\tilde{e}(p, y) = p \frac{1}{2} (y+1)^2 + (1-p) \left( \frac{1}{2} y^2 + v_0 \right) \quad (21)$$

Due to permutational invariance we can write the probability of a given state with  $p$  element in the post-power-stroke state in the form

$$\tilde{\rho}(p; y, \beta) = \frac{1}{Z(y, \beta)} \binom{N}{Np} \exp[-\beta N \tilde{e}(p; y, \beta)] \quad (22)$$

where  $Z(y, \beta) = \sum_{Np=0}^N \tilde{Z}(p; y, \beta)$  and

$$\tilde{Z}(p; y, \beta) = \binom{N}{Np} \exp[-\beta N \tilde{e}(p; y)]. \quad (23)$$

Alternatively, we can take advantage of the fact that our HS elements are independent and each of them has the distribution  $\rho_1$  given by (3). Therefore we can also write directly

$$\begin{aligned} \tilde{\rho}(p; y, \beta) &= \binom{N}{Np} [\rho_1(-1; y, \beta)]^{Np} [\rho_1(0; y, \beta)]^{N(1-p)} \\ &= \frac{1}{2^N} \binom{N}{Np} \left\{ 1 - \tanh \left[ \frac{\beta}{2} (y - y_0) \right] \right\}^{Np} \\ &\quad \times \left\{ 1 + \tanh \left[ \frac{\beta}{2} (y - y_0) \right] \right\}^{N(1-p)}. \end{aligned} \quad (24)$$

We again see that in the state of isometric contractions  $y = y_0$  the distribution  $\tilde{\rho}(p; y, \beta) = \binom{N}{Np} / 2^N$  is independent of temperature (given that it is finite). We reiterate that this can be viewed as an indication of the robustness of fluctuations in this physiologically most important state.

The probability density (24) can also be written as  $\tilde{\rho}(p; y, \beta) = [1/Z(y, \beta)] \exp[-\beta N \tilde{f}(p; y, \beta)]$  where the marginal free energy of the system at constant  $p$  reads

$$\tilde{f}(p; y, \beta) = -\frac{1}{N\beta} \ln(\tilde{Z}) = \tilde{e}(y, p) - \frac{1}{\beta} \tilde{s}(p). \quad (25)$$

Here  $\tilde{e}$  is the internal energy (21) and

$$\tilde{s}(p) = \frac{1}{N} \log \binom{N}{Np}$$

is the entropy at fixed  $p$ . In the limit  $N \rightarrow \infty$  we can obtain an explicit expression for the marginal free energy

$$\tilde{f}_\infty(p; y, \beta) = \tilde{e}(y, p) - (1/\beta) \tilde{s}_\infty(p), \quad (26)$$

where  $\tilde{s}_\infty$  is the ideal mixing entropy (elements do not interact),

$$s_\infty = -[p \log(p) + (1-p) \log(1-p)]. \quad (27)$$

The function  $\tilde{f}_\infty(p)$  is always convex because

$$\frac{\partial^2}{\partial p^2} \tilde{f}_\infty(p; y, \beta) = [\beta p(1-p)]^{-1} > 0. \quad (28)$$

The average value of the parameter  $p$  (which is analogous to the variable  $n_2$  in [5]) can be written as

$$\begin{aligned} \langle p \rangle(y, \beta) &= \sum p \tilde{\rho}(p; y, \beta) = -\langle x \rangle(y, \beta) \\ &= \frac{1}{2} \left\{ 1 - \tanh \left[ \frac{\beta}{2} (y - y_0) \right] \right\}, \end{aligned} \quad (29)$$

It plays the role of the average magnetization per spin and does not depend on  $N$ . We can also compute higher moments of the distribution  $\tilde{\rho}$ . In particular, we can write

$$\begin{aligned} N \langle [p - \langle p \rangle(y, \beta)]^2 \rangle &= \rho_1(-1; y, \beta) \rho_1(0; y, \beta) \\ &= \langle [x - \langle x \rangle(y, \beta)]^2 \rangle \\ &= \frac{1}{4} \operatorname{sech}^2 \left[ \frac{\beta}{2} (y - y_0) \right], \end{aligned} \quad (30)$$

implying that

$$\sqrt{\langle [p - \langle p \rangle(y, \beta)]^2 \rangle} = \frac{1}{2\sqrt{N}} \operatorname{sech} \left[ \frac{\beta}{2} (y - y_0) \right],$$

decays in the thermodynamic limit as  $N^{-1/2}$ . By differentiating Eq. 29 with respect to  $y$  we obtain the equilibrium susceptibility  $X$

$$\begin{aligned} X(y, \beta) &= -\frac{\partial}{\partial y} \langle p \rangle(y, \beta) \\ &= \beta N \langle [p - \langle p \rangle(y, \beta)]^2 \rangle \\ &= \chi(y, \beta), \end{aligned} \quad (31)$$

where

$$\chi(y, \beta) = \frac{\beta}{4} \operatorname{sech}^2 \left[ \frac{\beta}{2} (y - y_0) \right],$$

is the susceptibility of the single HS element, see Eq. 6.

The knowledge of the marginal free energy  $\tilde{f}(p; y, \beta)$  allows one to compute the equilibrium free energy

$$F(y, \beta) = -\frac{1}{\beta} \log \left\{ \sum_{Np=0}^N \exp \left[ -\beta N \tilde{f}(p; y, \beta) \right] \right\}. \quad (32)$$

Various finite size effects described by this formula are illustrated in Appendix C. In the limit  $N \rightarrow \infty$ , the summation over the set of discrete values of  $p$  can be transformed into an integral over the interval  $[0, 1]$  which,

in turn, can be computed using Laplace method. We obtain

$$F_\infty(y, \beta) = N \tilde{f}_\infty(p_*(y, \beta); \beta), \quad (33)$$

where  $\tilde{f}_\infty$  is given by Eq. 26 and  $p_*(y, \beta)$  is a minimizer of  $\tilde{f}_\infty$ , solution of the transcendental equation,

$$p_*/(1-p_*) = \exp[-\beta(y-y_0)]. \quad (34)$$

It is easy to check that  $p_*(y, \beta) = \langle p \rangle(y, \beta)$  and  $F_\infty(y, \beta) = N f(y, \beta)$  where  $\langle p \rangle(y, \beta)$  and  $f$  given by Eq. 29 and Eq. 8, respectively. Since the marginal energy is always convex, it has a single minimum  $p_*(y, \beta)$  which is a solution of Eq. 34, corresponding to a microscopic mixture involving folded and unfolded elements. In particular, for  $y = y_0$  where  $\langle p \rangle = 1/2$ , the system is maximally disordered with equal number of elements in both states.

Using Eqs. 29 and 30, and following Section II, we can now rewrite all the thermodynamic characteristics of the system in terms of the statistical properties of the order parameter  $p$  by replacing  $\langle x \rangle$  by  $-\langle p \rangle$  and  $\langle [x - \langle x \rangle(y, \beta)] \rangle$  by  $N \langle [p - \langle p \rangle(y, \beta)]^2 \rangle$ .

### C. Mechanical behavior

For a given configuration  $\mathbf{x}$ , the tension in the system is defined by the formula

$$\Sigma(\mathbf{x}, y) = N \left[ y - \frac{1}{N} \sum x_i \right] = N(y + p), \quad (35)$$

and then the expression for the average tension, conjugate to the control parameter  $y$ , can be written as

$$\langle \Sigma \rangle(y, \beta) = N [y + \langle p \rangle(y, \beta)] = N \langle \sigma \rangle(y, \beta), \quad (36)$$

where  $\langle \sigma \rangle$  is the average tension obtained for a single element, see Eq. 9. In the skeletal muscle framework this relation establish a direct connection between the observable fluctuations of the macroscopic tension and the fluctuations of the cross-bridges configuration at the nano-scale which can be recorded independently by using advanced optical techniques [49].

In addition to computing the average tension  $\langle \Sigma \rangle(y, \beta)$  we can also compute its variance explicitly

$$\begin{aligned} \langle [\Sigma - \langle \Sigma \rangle(y, \beta)]^2 \rangle &= N^2 \langle [p - \langle p \rangle(y, \beta)]^2 \rangle \\ &= N \langle [x - \langle x \rangle(y, \beta)]^2 \rangle \\ &= N \langle [\sigma - \langle \sigma \rangle(y, \beta)]^2 \rangle. \end{aligned} \quad (37)$$

The relative fluctuations of tension can be then presented in the form

$$\frac{\sqrt{\langle [\Sigma - \langle \Sigma \rangle(y, \beta)]^2 \rangle}}{\langle \Sigma \rangle(y, \beta)} = \frac{1}{\sqrt{N}} \frac{\sqrt{\langle [\sigma - \langle \sigma \rangle(y, \beta)]^2 \rangle}}{\langle \sigma \rangle(y, \beta)}. \quad (38)$$

We see that the relative fluctuations decay as  $1/N^{1/2}$  in accordance with classical statistical mechanics and the same type of decay can be also shown for the fluctuations of the other extensive quantities. For instance, if we denote by  $K$  the total stiffness of the system, we can write

$$\begin{aligned} K(y, \beta) &= N\kappa(y, \beta) \\ &= N \left[ 1 - \beta N \left\langle [p - \langle p \rangle (y, \beta)]^2 \right\rangle \right] \\ &= N - \beta \left\langle [\Sigma - \langle \Sigma \rangle (y, \beta)]^2 \right\rangle \end{aligned} \quad (39)$$

where  $\kappa$  is the stiffness of a single HS element, see Eq. 10. We see again again that the total stiffness decomposes into an elastic (or enthalpic) contribution dominating at  $|y - y_0| \gg 1$  and a term containing entropic contribution which dominates around  $y = y_0$ . If we rewrite Eq. 39 in dimensional quantities we obtain

$$\bar{K} = N\bar{\kappa}_0 - \frac{1}{k_b T} \left\langle [\bar{\Sigma} - \langle \bar{\Sigma} \rangle]^2 \right\rangle. \quad (40)$$

From this relation, we see that if the number of HS elements in the system is known and we have access to tension fluctuations, we can recover the stiffness of a single element  $\bar{\kappa}_0$  or conversely, knowing  $\bar{\kappa}_0$  we can estimate  $N$  by measuring the overall stiffness. Notice also that Eq. 40 can be tested at various  $\bar{y}$  and  $T$  allowing one to track the number of the attached elements at different degrees of stretching and different temperatures.

#### D. Thermal behavior

From the definition we write

$$S(y, \beta) = -\beta \frac{\partial}{\partial \beta} \log [Z(y, \beta)] + \log [Z(y, \beta)]$$

and since  $Z = Z_1^N$ , we obtain again that

$$S(y, \beta) = Ns(y, \beta).$$

This is another manifestation of the fact that macroscopic properties for the bundle of parallel HS elements can be obtained by simple rescaling of the same properties for a single element. We can then write similar expressions for the average energy,

$$\langle E \rangle (y, \beta) = N \langle v \rangle (y, \beta)$$

with  $\langle v \rangle$  given by Eq. 13; and its fluctuations

$$\left\langle [E - \langle E \rangle (y, \beta)]^2 \right\rangle = N \left\langle [v - \langle v \rangle (y, \beta)]^2 \right\rangle$$

with  $\left\langle [v - \langle v \rangle (y, \beta)]^2 \right\rangle$  given by Eq. 14. Similar expression can be written for the specific heat  $C(y, \beta) = Nc(y, \beta)$  where  $c(y, \beta)$  is given by Eq. 15. By linking the

fluctuations of the macroscopic tension with the fluctuations of the microscopic configuration ( see Eq. 37) we obtain

$$\begin{aligned} C(y, \beta) &= [N\beta(y - y_0)]^2 \left\langle [p - \langle p \rangle]^2 \right\rangle \\ &= [\beta (y - y_0)]^2 \left\langle [\Sigma - \langle \Sigma \rangle (y, \beta)]^2 \right\rangle. \end{aligned} \quad (41)$$

We also remark that the study of the adiabatic response for a single HS element in Section IID remains valid for the bundle of  $N$  HS elements.

To summarize, we have shown that the HS model can be mapped onto a paramagnetic spin system with the average conformation being the analog of magnetization. It belongs to the class of mean-field systems and its behavior is independent of dimensionality. This explains why the HS description of stochastic many body problem in terms of a chemical reaction with a single degree of freedom was so successful. For instance, their zero dimensional model could correctly account for the presence of series springs connecting the spins to the loading device and introducing such metamaterial features of the model as negative stiffness below the critical temperature  $\beta = 4$ . However, our detailed study of the equilibrium properties of the model shows that the chemo-mechanical description of Huxley and Simmons has its limitations. Thus, it deals with averages and ignores fluctuations and, more importantly, neglects the thermal effects. For instance, it remains oblivious to the fact that in the mechanics of skeletal muscles the state of isometric contractions has a maximal entropy and is robust to temperature changes. It also does not see the possibility that the first “elastic” phase of the quick recovery experiments, usually interpreted as *nonequilibrium* and *isothermal*, can in fact correspond to *equilibrium* and *adiabatic* response of the same system. These observations reveal additional “dimensions” of the HS model and suggest new experimental protocols focusing on the study of fluctuations and coupling mechanical and calorimetric measurements.

#### IV. KINETICS

In the two previous Sections we have studied equilibrium properties of the HS model, however, we did not specify the dynamics allowing the system to reach and maintain the thermodynamic equilibrium. An example of such dynamics was provided in the original paper of Huxley and Simmons [5] which modeled it as a first order chemical reaction and introduce an ODE describing the evolution of the average population of elements in two conformational states. In the HS model the loading was allowed to vary with time while the temperature was kept constant. In this Section we re-derive the kinetic model of Huxley and Simmons from a more general perspective of collective stochastic dynamics in the energy landscape characterizing the bundle of  $N$  HS elements connected in parallel.

### A. The model

In our stochastic model we have to deal with dynamics of individual bi-stable elements. Since the associated phase space is discrete, the dynamics of the microscopic variables  $x_i$  will consist of a series of jumps and we need to introduce the probabilities of the direct and reverse conformational changes in the time interval  $dt$

$$\begin{aligned} \mathbb{P}(x_i(t+dt) = -1 | x_i(t) = 0) &= k_+(y, \beta) dt \\ \mathbb{P}(x_i(t+dt) = 0 | x_i(t) = -1) &= k_-(y, \beta) dt. \end{aligned} \quad (42)$$

Here  $k_+(y, \beta)$  (resp.  $k_-(y, \beta)$ ) is the transition rate for the jump from the unfolded state (resp. folded state) to the folded state (resp. unfolded state) and the total elongation  $y$  and the inverse temperature  $\beta$  remain to be the controlling parameters that may also vary with time with a rate that is sufficiently slow comparing to the rate of the individual conformational transitions. As the transition probabilities (42) depend in this model only on the current state of the system, the stochastic process describing the transitions of a single element as a discrete Markov chain [44, 66]. The presence of the jumps is a shortcoming of the spin model and in the model with non-degenerate elastic bi-stable elements they need to be replaced by a continuous Langevin dynamics [40, 41].

To compute the transition rates  $k_{\pm}(y, \beta)$  we need to say something about the structure of the energy landscape separating the two conformational states. In view of the jump nature of our dynamics it is sufficient to prescribe the height of the energy barrier. Following [5] we simply add the elastic energy of the linear spring to the height of the flat microscopic energy barrier assumed to be the same for each bi-stable element, see Fig. 7(a,b) for the notations. Assuming a flat barrier imposes the relation  $E_1 = E_0 + v_0$  to maintain the continuity of the energy landscape. Hence only one additional parameter (*e.g.*  $E_1$ ) is required to describe kinetics. When the height of both barriers  $E_0$  and  $E_1 = E_0 + v_0$  is large compared to  $kT$  we can use the Kramers approximation and write the transition rates in the form

$$\begin{aligned} k_+(y, \beta) &\propto \exp\left[-\beta \left[ E_0 + \max\left\{ \frac{1}{2}(y+1)^2 - \frac{1}{2}(y)^2, 0 \right\} \right]\right] \\ k_-(y, \beta) &\propto \exp\left[-\beta \left[ E_1 + \max\left\{ \frac{1}{2}(y)^2 - \frac{1}{2}(y+1)^2, 0 \right\} \right]\right]. \end{aligned}$$

Notice that Huxley and Simmons [5] considered only the case when  $1/2(y+1)^2 - 1/2(y)^2 > 0$ , implying  $y > -1/2$ . To see why the value  $y = -1/2$  is special we recall that for the unloaded system we assumed that  $\langle p \rangle = 1/2$  and since during the purely elastic phase the fraction of folded elements does not change, the shortening required in such system to reach zero tension is exactly  $y = -1/2$ . In most experiments on muscles, the relaxation rates are measured for  $y > -1/2$  because below this threshold the muscle fiber is likely to buckle.

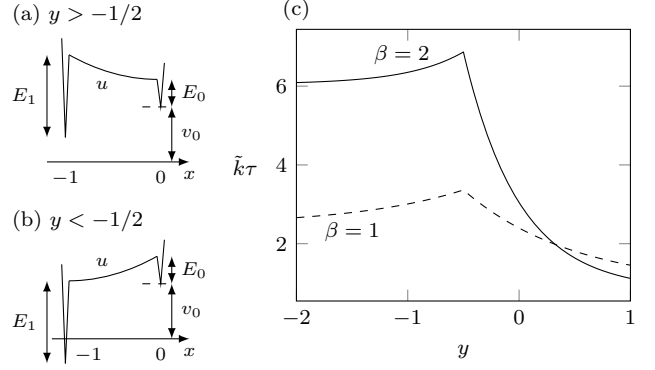


FIG. 7. Schematic representation of the energy barrier in the HS bistable potential. The energy barriers corresponding to the transition rates in the absence of elastic contribution are denoted  $E_1$  and  $E_2$ . We define the characteristic timescale by  $\tau = 1/\exp[\beta E_1]$ . (a) Energy landscape for  $y > -1/2$  which is the case considered in [5]; (b) Energy landscape for  $y < -1/2$  not considered by Huxley and Simmons. (c), Relaxation rate as function of the total elongation  $y$  for  $\beta = 1$  (dashed line) and  $\beta = 2$  (solid line).

For  $y > -1/2$  only the energy barrier from the unfolded to the folded state depends on  $y$ , see Fig. 7(a). In this case, the rates become

$$k_+(y, \beta) = k_- \exp[-\beta(y - y_0)], \quad (43)$$

$$k_-(y, \beta) = \exp[-\beta E_1] = \text{const.} \quad (44)$$

and it is  $k_-$  which determines the timescale of the dynamic response namely

$$\tau = 1/k_- = \exp[\beta E_1].$$

One can see that it is fully controlled by a single parameter  $E_1$  whose value was chosen by Huxley and Simmons to match their observations.

The possibility that  $y < -1/2$  was not considered in [5]. In this case the barriers are

$$k_+(y, \beta) = \exp[-\beta E_0] = \text{const.}$$

$$k_-(y, \beta) = k_+ \exp[\beta(y - y_0)]$$

and only the reverse transition rate depends on  $y$ , see Fig. 7(b).

The dependence of the relaxation rate  $\tilde{k} = k_+ + k_-$  on the total elongation is illustrated in Fig. 7(c). The relaxation rate reaches its maximum at  $y = -1/2$  where the kinetics switches from the regime where only the folding barrier depends on the loading ( $y > -1/2$ ) to the regime where only the unfolding barrier depends on the loading ( $y < -1/2$ ). For  $y < -1/2$  the elastically deformed system is in compression before the beginning of relaxation and the relaxation rate decreases with the loading (catch bond type behavior) which may be of interest outside the context of skeletal muscles [67, 68].

The isothermal stochastic dynamics of the system specified by the transition rates (43,44) can be also described

in terms of the probability density  $\tilde{\rho}(p, t; y, \beta)$  which satisfies the Master Equation,

$$\begin{aligned} \frac{\partial}{\partial t} \tilde{\rho}(p, t; y, \beta) &= \phi_+(1 - p + 1/N; y) \tilde{\rho}(p - 1/N, t; y, \beta) \\ &+ \phi_-(p + 1/N; y) \tilde{\rho}(p + 1/N, t; y, \beta) \\ &- [\phi_+(1 - p; y) + \phi_-(p; y)] \tilde{\rho}(p, t; y, \beta) \end{aligned} \quad (45)$$

where  $\phi_+(p; y) = (1 - p)k_+(y)$  and  $\phi_-(p; y) = pk_-(y)$ . This equation is compatible with the HS kinetic equation describing the evolution of the first moment of the distribution  $\langle p \rangle = \sum p \rho(p, t; z, \beta)$

$$\begin{aligned} \frac{\partial}{\partial t} \langle p \rangle(t; y, \beta) &= \langle \phi_+(1 - p; y) \rangle - \langle \phi_-(p; y) \rangle \\ &= k_+(y)(1 - \langle p \rangle) - k_-(y)\langle p \rangle. \end{aligned} \quad (46)$$

Equation (46) could also be derived directly if we noticed that since the elements are independent in the hard device case  $\langle p \rangle(t + dt) = \mathbb{P}(x = -1, t + dt)$ . Then, using transition probabilities (42) we obtain

$$\begin{aligned} \mathbb{P}(x = -1, t + dt) &= k_+(y)[1 - \mathbb{P}(x = -1, t)]dt \\ &+ [1 - k_-(y)dt]\mathbb{P}(x = -1, t). \end{aligned}$$

and then by taking the limit  $dt \rightarrow 0$  we obtain (46). The advantage of the more complete description of dynamics in terms of the Master Equation (45) is that in addition to averages, one can also follow evolution of the higher moments.

## B. Quasi-static loading

To make sure that our dynamical model is compatible with the equilibrium behavior of the system studied in Section II, we first study the case of quasi-static driving of the system through the control parameter  $y$  with the temperature remaining constant. While this loading protocol may be not very relevant in the case of skeletal muscles because of the involvement at these rates of the ATP driven processes, it is of great relevance in the modeling of unzipping tests for various biological macromolecules [23, 26, 29, 69].

The stationary solution of Eq. 45 can be written explicitly [44, 66]

$$\tilde{\rho}_\infty(p; y, \beta) = \frac{\prod_{Np=1}^{Np} \frac{\phi_+(i-1/N; y, \beta)}{\phi_-(i; y, \beta)}}{1 + \sum_{Nj=0}^N \prod_{Ni=1}^{Nj} \frac{\phi_+(i-1/N; y, \beta)}{\phi_-(i; y, \beta)}} \quad (47)$$

and for the rates given by Eq. 43 and 44 we have

$$\frac{\phi_+(p - 1/N; y, \beta)}{\phi_-(p; y, \beta)} = \frac{1 - p + 1/N}{p} \exp[-\beta(y - y_0)], \quad (48)$$

In this case (47) can be rewritten as

$$\rho_\infty(p; y, \beta) = \frac{\binom{N}{Np} \exp[-\beta Np(y - y_0)]}{1 + \sum_{Nj=0}^N \binom{N}{Nj} \exp[-\beta Nj(y - y_0)]}. \quad (49)$$

and noticing that  $p(y - y_0) = \tilde{e}(p; y) - y^2/2 - v_0$ , we finally obtain

$$\rho_\infty(p; y, \beta) = \frac{\binom{N}{Np} \exp[-\beta N\tilde{e}(p; y)]}{\sum_{Nj=0}^N \binom{N}{Nj} \exp[-\beta N\tilde{e}(j; y)]}.$$

This expression for the stationary probability distribution is equivalent to Eq. 24. Similarly, the stationary solution of the HS kinetic Eq. 46

$$\langle p \rangle_\infty = \frac{k_+(y, \beta)}{k_+(y, \beta) + k_-(y, \beta)} \quad (50)$$

becomes equivalent to Eq. 29 after the substitution of expressions for the rates (43) and (44).

The behavior of the individual trajectories generated by our stochastic model in quasi-static loading conditions is illustrated in Fig. 8 where we show the response of a system with  $N = 10$  (light grey) and  $N = 100$  (dark grey) elements subjected to continuous stretching from  $y = y_0 - 1$  to  $y = y_0 + 1$  over the time interval  $[0, 100\tau]$ . The stochastic trajectories were modeled by Gillespie algorithm [70]. It involves the computation of the time of the next transition event which is a random variable with an exponential distribution depending on the current state followed by the selection of the transition to occur at this time. In our case, the first step of the algorithm uses the current value of the control parameter  $y$ . Therefore, the computation of the time of next transition assumes that the timescale associated with the variable  $y$  is large compared to the average time between two transition events so that  $y$  can be considered constant between the events.

The evolution of the order parameter  $p$  is represented in (a-c) while the corresponding tension curves are shown in (d-f). The stochastic dynamics, is compared with the corresponding equilibrium response curves implying averaging over individual trajectories and accessible by means of the chemo-mechanical model of Huxley and Simmons (thick lines).

The salient feature of the stochastic trajectories for the HS system with a realistic (small) number of elements, shown in Fig. 8, is their noisiness. A closer look reveals a succession of jumps describing individual folding-unfolding events as it is suggested by the model at finite  $N$ , see Appendix C. As the number of element increases the fluctuations of  $p$  decrease which is in accordance with our Eq. 30, and a single realisation trajectory (dark grey) gets close to the average trajectory even though some steps can still be occasionally observed. The insets in Fig. 8(d-e) illustrate the equilibrium distribution  $\tilde{\rho}(p; y, \beta)$  obtained from 1000 realizations of the stochastic process with solid line depicting the analytic solution given by Eq. 19. Expectantly, the distribution does not depend on the temperature at  $y = y_0$  while becoming progressively more localized away from this point. Overall the equilibrium distribution of the order parameter  $p$  given by Eq. 24 gets sharply peaked around its mean as the number of elements  $N$  increases.

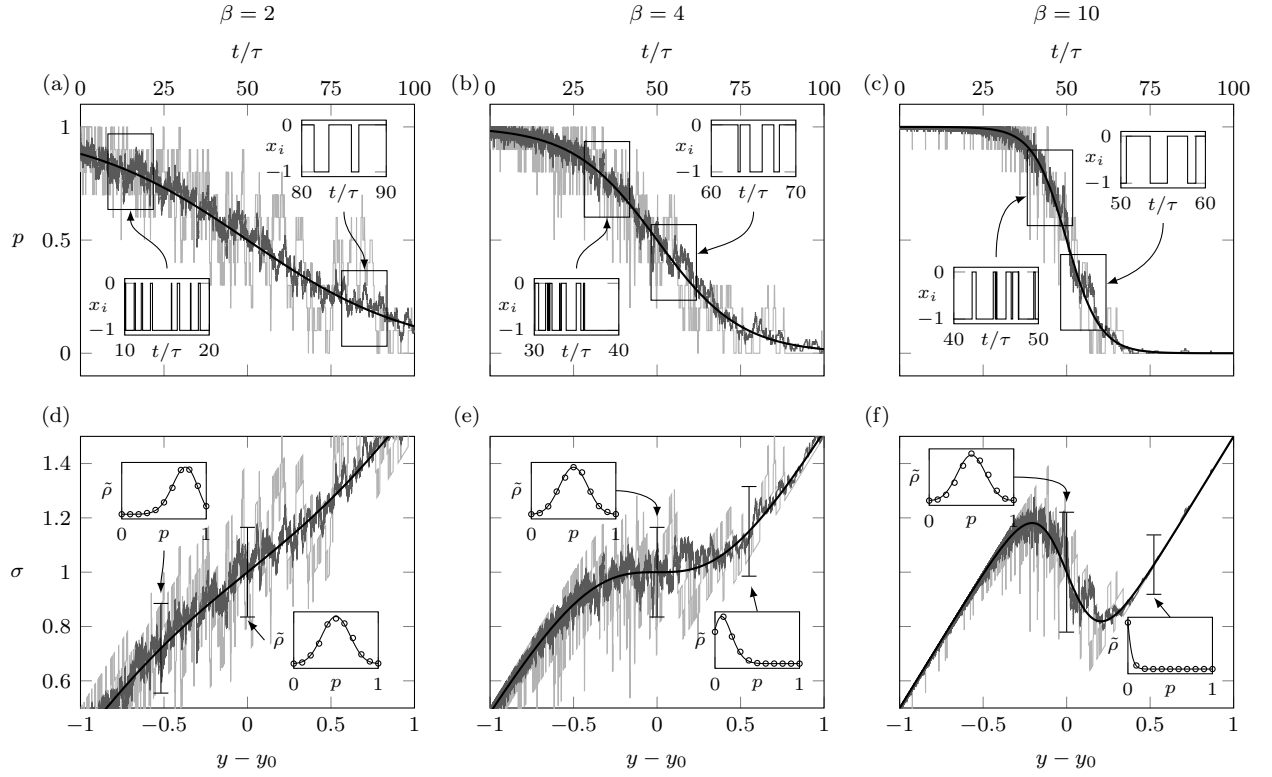


FIG. 8. Quasi-static response of the HS model to the abrupt loading from  $y_0 - 1$  to  $y_0 + 1$  achieved in  $100\tau$ . Individual stochastic trajectories are shown for  $N = 10$  (light grey) and  $N = 100$  (dark grey). Left,  $\beta = 2$ ; center,  $\beta = 4$  and right,  $\beta = 10$ . (a-c) Evolution of the order parameter  $p$ . The inserts show two samples of a single trajectory around the point where  $p = 1/2$ . (d-f), Tension-elongation relation obtained from  $\sigma = y + p$ . The inserts show the marginal distribution  $\hat{\rho}$  at the two different times indicated by the vertical bars. Bold lines represent the thermal equilibrium averages given by Eq. 29 and Eq. 9

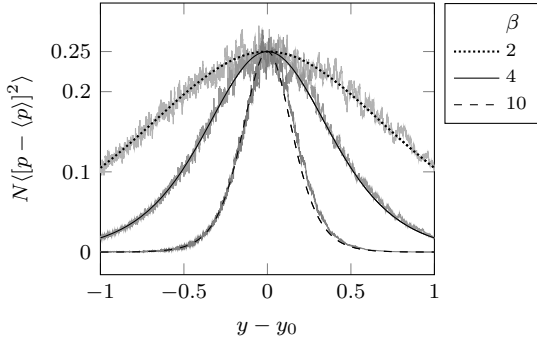


FIG. 9. Evolution of  $\langle p \rangle$  (a) and of the normalized variance  $N \langle (p - \langle p \rangle)^2 \rangle$  (b) as function of the elongation during a quasi-static stretching between  $t = 0$  and  $t/\tau = 100$  for different values of the temperature. For each temperature we superimpose the analytic computations from Eq. 29 and Eq. 30 and the numerical results corresponding to 1000 independent realisations with  $N = 100$ . Dotted line,  $\beta = 2$ ; solid line,  $\beta = 4$ ; dashed line,  $\beta = 10$ .

The sample trajectories of individual bi-stable elements, constantly switching between the unfolded  $x_1 = 0$  and folded  $x_1$  states, are illustrated in the inserts included into Fig. 8(a-c). To make these stochastic fluctu-

ations more visible, we compare in Fig. 9 the variance of the order parameter  $p$  obtained from the stochastic model with the results of the analytic computations based on Eq. 30. The system contains  $N = 100$  elements and each stochastic trajectory corresponds to 1000 realizations of our Markov process. We see that stochastic simulations are fully compatible with the predictions of equilibrium theory, in particular, we see once again that the normalized variance at  $y = y_0$  is independent of the temperature. However, the simulations also reveal unavoidable fluctuations that are particularly strong around the “critical” point  $y = y_0$  and  $\beta = 4$ . The functional role of these fluctuations, that are obviously out of reach for the quasi-chemical models, remains to be understood.

### C. Fast loading

The ultimate test of the dynamical model is when the system responds to abrupt perturbations. Since this is exactly the type of mechanical tests conducted by HS in their seminal paper [5], it is instructive to consider the response of the HS system to such perturbations in the framework of our more detailed stochastic description.

For  $N$  HS elements connected in parallel, stochastic

evolution of the macroscopic quantity  $p(t)$  is governed by the jump probabilities

$$\mathbb{P}\left[p(t+dt) = p + \frac{1}{N} \middle| p(t) = p\right] = (1-p)k_+(y, \beta)dt \quad (51)$$

$$\mathbb{P}\left[p(t+dt) = p - \frac{1}{N} \middle| p(t) = p\right] = pk_-(y, \beta)dt. \quad (52)$$

The stochastic trajectories were simulated again with Gillespie algorithm [70]. In this description temperature was treated as a silent parameter kept at a constant value. Hence, we could not model in this way potentially non-isothermal (say, adiabatic) processes discussed in Section IID.

In Fig. 10 we illustrate our stochastic model by showing the response of the system to a rapid shortening at  $\beta = 4$ . The system is first maintained in equilibrium at  $y = y_0 = 0.5$  before a rapid length change to  $y = 0$  is applied (at  $t = 0$ ). This protocol is repeated for systems with  $N = 10$  and  $N = 100$ . In Fig. 10 (a) and Fig. 10 (b), single trajectories are represented by dotted lines ( $N = 10$ ) and grey lines ( $N = 100$ ) while the solid black line shows the average response of the system with  $N = 10$ . The square symbols represent the response obtained using the HS reaction kinetic equation (46). Notice that, especially in the case  $N = 10$ , a single trajectory can be rather different from the average behavior predicted by the quasi-chemical model. Overall, we see that not only the averages of the measurable quantities but also their variance, characterising the scale of fluctuations, can be used as an indicator of the current state of the system.

In Fig. 11 we show how the probability distribution changes with time as the system is first driven out of equilibrium and then gradually recovers it. Since in the case of interest the parameter  $N$  is rather small, the self averaging does not take place and such information about the system cannot be captured by quasi-chemical models. The statistics predicted by the model can be in principle tested in experiment, for instance, in the transient states the probability distribution loses its Gaussian structure and this should be detectable through the measurements of the higher moments of the probability distribution.

An important remaining question is how to deal with isothermal-adiabatic dichotomy at the present level of the description of kinetics. The simplest possibility would be to use the adiabatic condition as a feedback between the mechanical state of the system and the temperature of the reservoir. Another way is to model more closely the conditions of thermal exchange of the system with its environment and consider the possibility when the external temperature characterising the heat bath and the internal temperature characterising our subsystem do not coincide. We leave these issues for a separate study.

## V. CONCLUSIONS

In this paper we presented a non-orthodox perspective on the seminal HS model of collective folding by viewing it through the prism of statistical mechanics. By placing the emphasis on fluctuations and thermal effects, that have been so far underplayed in the interpretation of the experiments, we challenged the exhaustiveness of the chemo-mechanical approach initiated by Huxley and Simmons and proposed new types of experimental protocols which combine mechanical and calorimetric testing.

Our analysis draws an analogy between the HS model in a *hard device* and the paramagnetic Ising model. The fact that the response of this multiparticle system can be understood by studying the behavior of a single element explains the effectiveness of the chemo-mechanical approach adopted by Huxley and Simmons. The HS system, however, is not fully identical to a paramagnet, in particular, it exhibits negative stiffness. It also shows anomalous fluctuations in a single point of the parameter space. The associated criticality is however fictitious since the marginal free energy in this model is always convex and the system does not exhibit any cooperativity.

The HS system in a hard device is different from a paramagnetic system because, rather unusually, the applied field is characterized by its own energy which brings into the system some additional external stiffness. When this positive external stiffness becomes equal to the (negative) internal stiffness, which carries a sizable entropic contribution, the system finds itself in the pseudo-critical point as in the case of van der Waals gas (ferromagnetic system) placed in a container with fixed volume.

Our conclusion about the de-synchronized behavior of individual HS elements contradicts the usual perception about correlated, collective response of such systems and it is clear that to generate coherency of the mechanical response an interaction between the elements is necessary. A long-range interaction among individual HS elements of the mean-field type is revealed already in the soft device loading (analog of controlled pressure) where one recovers cooperativity and observes the analog of spontaneous magnetization [41].

Some of the most interesting findings of this paper concern the relation between mechanical and thermal properties of the HS system and the link between the thermodynamic quantities and the fluctuations. For instance, our analysis sheds light on the previously unnoticed temperature robustness of the state of isometric contractions where specific heat vanishes and fluctuations become temperature independent. Our study also raises awareness about the possibility of considerable temperature variation during the experiments involving fast loading and shows that isothermal and adiabatic responses of the HS system to mechanical solicitations may be rather different.

We point that the pervasiveness of hopping between different configurations in the finite size HS system can

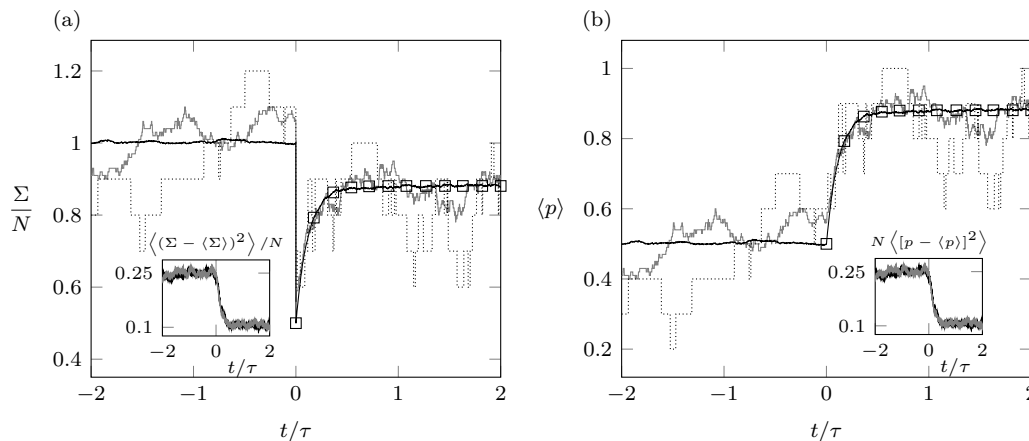


FIG. 10. Stochastic simulation of a quick force recovery in response of a step  $y - y_0 = -0.5$ . (a) tension per cross-linker; (b) average fraction of folded elements; (c), normalised fluctuations. In (a) and (b), dotted lines, single stochastic trajectory for a system with  $N = 10$ ; grey line single trajectory with  $N = 100$ ; solid line average over 1000 trajectories with  $N = 10$ ; squares, response obtained using HS kinetics, see Eq. 46. Inserts in (a), grey (resp. solid) line, fluctuations obtained using 1000 realisations for  $N = 100$  (resp.  $N = 10$ ). The inserts in (b) show the equilibrium distribution before and after the step. Parameters are  $\beta = 4$ ,  $v_0 = 1$ .

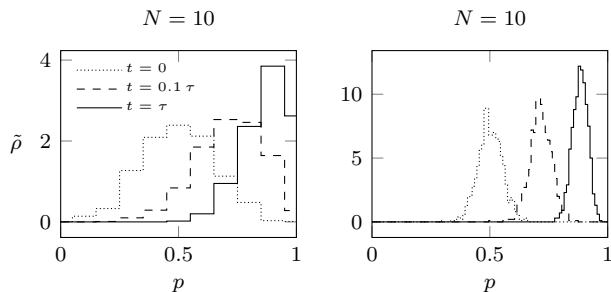


FIG. 11. Time evolution (snapshots) of the probability density  $\tilde{\rho}(p, t; y, \beta)$  showing gradual equilibration of the system subjected to an abrupt shortening. Parameters are the same as in Fig. 10

become a source of important information about the current state of such system. In relation to muscles, the stochastic perspective on fast force recovery allowed us to propose an explicit link between the intensity of force fluctuations, the effective stiffness and the number of the attached cross-bridges that can be tested in focused experiments.

The results obtained in the present paper are relevant for a large family of biological systems containing multi-stable units arranged in parallel. For instance the HS model has undergone reincarnation as a Bell model [20] describing the slip-bond behavior of cell-adhesion patches [71] and has been used almost verbatim in the theory of gating in hair cells [21]. The same formalism can also be used in the broad context of macromolecular folding [23, 26] including a mechanistic representation of a force behind the synaptic fusion pore opening (SNAREs proteins) [33].

Despite its versatility, the HS model has several serious

limitations. For instance, in the muscle context, it is well known that the filamental backbones connecting individual bi-stable elements are elastically compliant [56, 57]. If this effect is taken into consideration, the parallel force generating elements are no more independent. Similar observations can be made regarding the focal adhesion patches that are also elastic and the elasticity of macromolecules loaded through compliant optical traps. The mechanical feedback provided by backbone elasticity [41] implies various degrees of synchronization which can be identified already at zero temperature [42]. The detailed analysis of such ferromagnetic behavior at finite temperature will be given in a companion paper. Some other limitations of the HS model such as the oversimplification of the geometry of the power stroke mechanism and the neglect of ATP fueled “activity” have been addressed in [50].

## VI. ACKNOWLEDGMENTS

The authors thank R. Sheshka, F. Staniscia, P. Recho, T. Lelièvre and J.-M. Allain for helpful discussions.

### Appendix A: Domain with negative stiffness

Above the critical point we can define an interval  $[y_-, y_+]$  delimiting the domain where the stiffness of the system is negative, see the dots corresponding to  $\beta = 10$  in Fig. 3(c,d). The boundaries  $y_-$  and  $y_+$  correspond to the zeros of the second derivative of the free energy. For

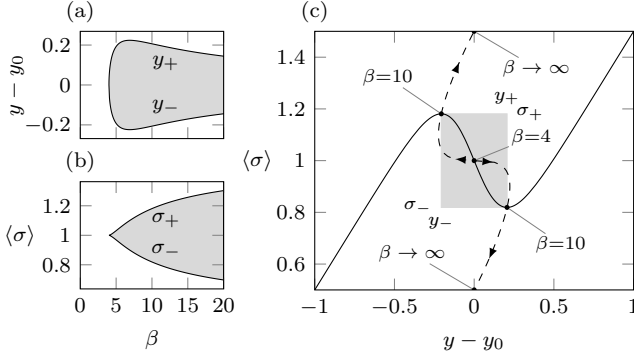


FIG. 12. Evolution of the domain of negative stiffness with temperature. (a) and (b) show the horizontal ( $y_+$  and  $y_-$ ) and vertical ( $\sigma_+$  and  $\sigma_-$ ) boundaries of the bistable domain. (b) dashed line, ( $y_-(\beta), \sigma_+(\beta)$ ) and ( $y_+(\beta), \sigma_-(\beta)$ ) represented for  $\beta = 4$  to  $\beta \rightarrow \infty$ . Solid line, tension-elongation relation corresponding to  $\beta = 10$ , the associated bi-stable domain is represented by the gray area. In this figure,  $v_0 = 1$ .

$\beta > 4$  we have

$$y_+(\beta) - y_0 = \frac{1}{\beta} \log \left[ \frac{\sqrt{\beta} + \sqrt{\beta - 4}}{\sqrt{\beta} - \sqrt{\beta - 4}} \right]$$

$$y_-(\beta) - y_0 = -\frac{1}{\beta} \log \left[ \frac{\sqrt{\beta} + \sqrt{\beta - 4}}{\sqrt{\beta} - \sqrt{\beta - 4}} \right]$$

In the zero temperature limit, we see that this interval collapses to a single point  $y = y_0$ . The equilibrium tensions  $\sigma_-$  and  $\sigma_+$  corresponding to  $y_+$  and  $y_-$ , respectively are given by

$$\sigma_+(\beta) = v_0 + \frac{1}{2} \sqrt{1 - 4\beta^{-1}} - \frac{1}{\beta} \log \left[ \frac{\sqrt{\beta} + \sqrt{\beta - 4}}{\sqrt{\beta} - \sqrt{\beta - 4}} \right]$$

$$\sigma_-(\beta) = v_0 - \frac{1}{2} \sqrt{1 - 4\beta^{-1}} + \frac{1}{\beta} \log \left[ \frac{\sqrt{\beta} + \sqrt{\beta - 4}}{\sqrt{\beta} - \sqrt{\beta - 4}} \right],$$

and become equal to  $\sigma_+ = v_0 + 1/2$  and to  $\sigma_- = v_0 - 1/2$ , when  $\beta \rightarrow \infty$ , respectively; see [42].

The evolution of the domain of negative stiffness is represented in Fig. 12. In (a) and (b) the boundaries  $y_{\pm}$  and  $\sigma_{\pm}$  are represented as function of temperature while in (c) we show the parametric plots ( $y_-(\beta), \sigma_+(\beta)$ ) and ( $y_+(\beta), \sigma_-(\beta)$ ) see dashed line.

### Appendix B: Average internal energy

The average internal energy of a single cross-linker is represented in Fig. 13 for different values of the temperature. In the zero temperature limit (dot-dashed line), the average internal energy coincides with the mechanical energy [42]. We see that for finite temperature, the average internal energy is strictly higher than the mechanical energy and decreases as temperature decreases. The situation is different for the free energy presented in Fig. 3. In this case, the free energy is always lower than

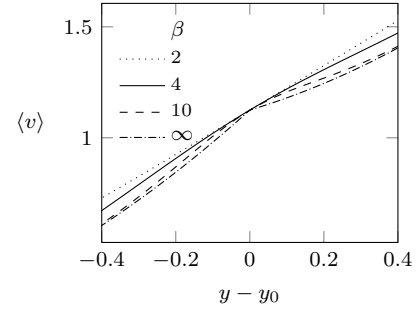


FIG. 13. Average internal energy for  $\beta = 2$  (dotted),  $\beta = 4$  (solid),  $\beta = 10$  (dashed) and in the athermal limit  $\beta \rightarrow \infty$  (dot-dashed). Here  $v_0 = 1$ .

the mechanical energy and increases as temperature decreases. Hence the average internal energy approaches the mechanical energy “from above” while the free energy approaches the mechanical energy “from below”.

### Appendix C: Representation of the marginal free energy

To illustrate our general formulas we consider here first the simplest case when  $N = 2$ . The marginal free energy can take three values,

$$\tilde{f}(0; y, \beta) = \tilde{v}(0; y) = \frac{1}{2}y^2 + v_0$$

$$\tilde{f}(1/2; y, \beta) = \frac{1}{4}(y+1)^2 + \frac{1}{4}y^2 + \frac{1}{2}v_0 - \frac{\log(2)}{2\beta}$$

$$\tilde{f}(1; y, \beta) = \tilde{v}(1; y) = \frac{1}{2}(y+1)^2,$$

which are represented by dotted lines on Fig. 14(a). Notice that the free energy of the homogeneous states coincide with the corresponding internal energy as the entropy vanishes for such states. In Fig. 14(b) the tension-elongation relations corresponding to the different free energy levels in Fig. 14(a) are represented by dotted lines and the tension-elongation corresponding to the global minimum is represented by the thick line.

Observe that the global minimum response at finite temperature is characterised by a series of jump corresponding to successive conformational changes in individual elements. Between the jumps, the stiffness is positive which shows that each metastable state has a finite interval of stability even though the global stiffness is negative. As the number of metastable states increases with  $N$  the tension-elongation curve become smoother. In the continuum limit  $N \rightarrow \infty$  the domain of the phase space occupied by the metastable states becomes compact, see gray area in Fig. 14 (e) and (f). The absence of interaction between the units leads to ideal mixing of folded and unfolded units which indicates the lack of synchronisation.

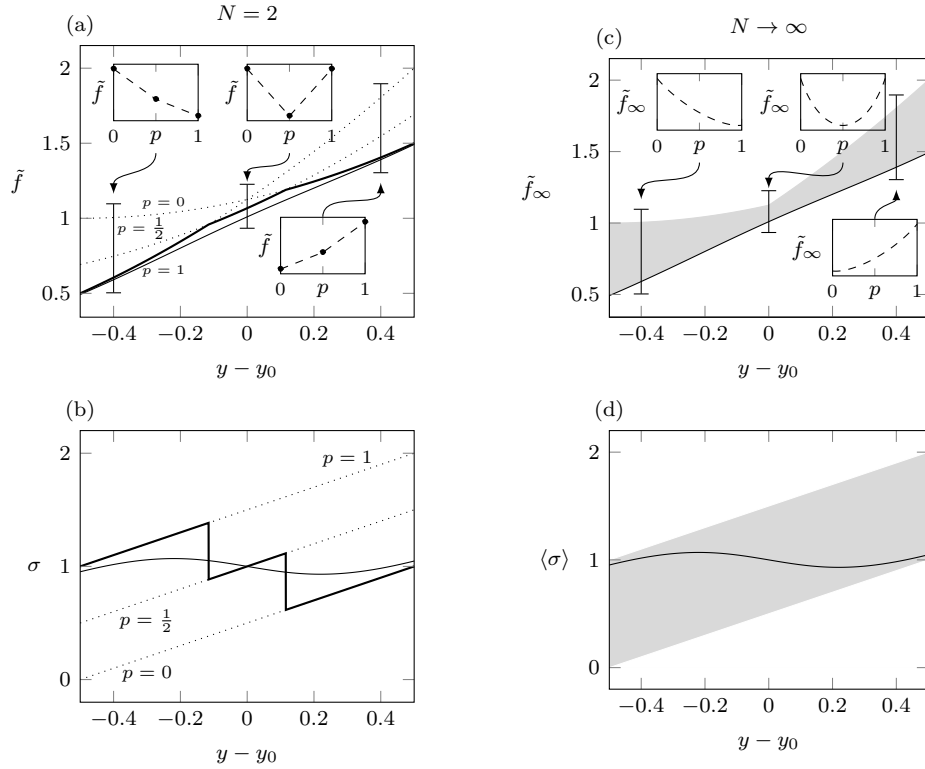


FIG. 14. Nonequilibrium free energy landscape and the corresponding tension-elongation relations in a hard device for  $N = 2$  (a,b) and in the limit  $N \rightarrow \infty$  (c,d). Dotted lines, free energy levels and tension corresponding to different values of  $p$ ; thick line, response corresponding to the global minimum of the nonequilibrium free energy; thin line, response in thermal equilibrium; grey areas, domain of the metastable states; thin lines, thermal equilibrium equilibrium free energy and corresponding tension-elongation relation. In (a),(c) and (e), the inserts show the marginal free energy  $\tilde{f}$  as function of  $p$  for  $y - y_0 = -0.4, 0, 0.4$ . The plots are obtained with  $\beta = 6$  which explains the presence of negative stiffness.

## REFERENCES

- 
- [1] R. Podolsky, *Nature* **188**, 666 (1960).  
[2] M. Civan and R. Podolsky, *Biophys. J.* **184**, 511 (1966).  
[3] R. Podolsky, A. C. Nolan, and S. A. Zaveler, *Proc. Natl. Acad. Sci. U.S.A.* **64**, 504 (1969).  
[4] A. F. Huxley and R. M. Simmons, *J. Physiol.* **208**, 52P (1970).  
[5] A. F. Huxley and R. M. Simmons, *Nature* **233**, 533 (1971).  
[6] K. Holmes and M. Geeves, *Philos. T. Roy. Soc. B* **355**, 419 (2000).  
[7] M. Linari, M. Caremani, and V. Lombardi, *P Roy. Soc. Lond. B Bio.* **277**, 19 (2010).  
[8] I. Rayment, H. Holden, M. Whittaker, C. Yohn, M. Lorenz, K. Holmes, and R. Milligan, *Science* **261**, 58 (1993).  
[9] R. Dominguez, Y. Freyzon, K. M. Trybus, and C. Cohen, *Cell* **94**, 559 (1998).  
[10] R. Lynn and E. Taylor, *Biochemistry* **10**, 4617 (1971).  
[11] B. Alberts, A. Johnson, J. Lewis, M. Raff, K. Roberts, and P. Walter, *Molecular Biology of the Cell*, 5th ed. (Garland Science, New York, 2007).  
[12] T. Erdmann and U. S. Schwarz, *Biophys. J.* **91**, L60 (2006).  
[13] T. Erdmann and U. S. Schwarz, *Eur. Phys. J.* **22**, 123 (2007).  
[14] T. Erdmann and U. Schwarz, *Phys. Rev. Lett.* **108**, 188101 (2012).  
[15] T. L. Hill, *Prog. Biophys. Molec. Biol.* **28**, 267 (1974).  
[16] T. L. Hill, *Prog. Biophys. Molec. Biol.* **29**, 105 (1976).  
[17] A. F. Huxley and S. Tideswell, *J. Muscle Re. Cell M.* **17**, 507 (1996).  
[18] G. Piazzesi and V. Lombardi, *Biophys. J.* **68**, 1966 (1995).  
[19] D. Smith, M. Geeves, J. Sleep, and S. Mijailovich, *Ann. Biomed. Eng.* **36**, 1624 (2008).  
[20] G. Bell, *Science* **200** (1978).  
[21] J. Howard and A. J. Hudspeth, *Neuron* **1**, 189 (1988).  
[22] P. Martin, A. Mehta, and A. Hudspeth, *Proc. Natl. Acad. Sci. USA* **97**, 12026 (2000).  
[23] J. Liphardt, B. Onoa, S. B. Smith, I. Tinoco, and C. Bus-

- tamante, *Science* **292**, 733 (2001).
- [24] N. Bosaeus, A. H. El-Sagheer, T. Brown, S. B. Smith, B. Åkerman, C. Bustamante, and B. Norden, *Proc. Natl. Acad. Sci. U.S.A.* **109**, 15179 (2012).
- [25] M. T. Woodside, C. Garcia-Garcia, and S. M. Block, *Curr. Opin. Chem. Biol.* **12**, 640 (2008).
- [26] A. N. Gupta, A. Vincent, K. Neupane, H. Yu, F. Wang, and M. T. Woodside, *Nature* **7**, 631 (2011).
- [27] A. Prados, A. Carpio, and L. L. Bonilla, *Phys. Rev. E* (2012).
- [28] V. Muñoz, E. R. Henry, J. Hofrichter, and W. A. Eaton, *Proc. Natl. Acad. Sci. U.S.A.* **95**, 5872 (1998).
- [29] T. Bornschlögl and M. Rief, *Physical Review Letters* (2006).
- [30] A. Srivastava and R. Granek, *Phys. Rev. Lett.* **110**, 138101 (2013).
- [31] U. Gerland, R. Bundschuh, and T. Hwa, *Biophysj* **84**, 2831 (2003).
- [32] N. Thomas and Y. Imafuku, *J Theor Biol* (2012).
- [33] T. C. Südhof, *Neuron* **80**, 675 (2013).
- [34] L. L. Bonilla, A. Carpio, A. Prados, and R. R. Rosales, *Phys. Rev. E* **85**, 031125 (2012).
- [35] A. Vilfan and T. Duke, *Biophys. J.* **85**, 818 (2003).
- [36] K. Kruse and F. Jülicher, *Curr. Opin. Cell Biol.* **17**, 20 (2005).
- [37] A. Vilfan and E. Frey, *J. Phys.: Condens. Matter* **17**, S3901 (2005).
- [38] T. Guerin, J. Prost, P. Martin, and J.-F. Joanny, *Curr. Opin. Cell Biol.* **22**, 14 (2010).
- [39] R. Balian, *From Microphysics to Macrophysics*, Methods and Applications of Statistical Physics (Springer Science & Business Media, 2006).
- [40] L. Marcucci and L. Truskinovsky, *Phys. Rev. E* **81** (2010).
- [41] M. Caruel, J. M. Allain, and L. Truskinovsky, *Phys. Rev. Lett.* **110**, 248103 (2013).
- [42] M. Caruel, J.-M. Allain, and L. Truskinovsky, *J. Mech. Phys. Solids* **76**, 237 (2015).
- [43] C. Gardiner, *Handbook of stochastic methods for physics chemistry and the natural sciences*, 3rd ed. (Springer, 2004).
- [44] T. Erdmann, P. J. Albert, and U. S. Schwarz, *J. Chem. Phys.* **139**, 175104 (2013).
- [45] C. F. Armstrong, A. F. Huxley, and F. J. Julian, *J. Physiol. - London*, 26 (1966).
- [46] K. A. P. Edman, *J. Physiol. - London* **404**, 301 (1988).
- [47] H. Granzier, A. Mattiazzi, and G. Pollack, *Am. J. Physiol.* **259**, C266 (1990).
- [48] K. A. P. Edman and N. Curtin, *J. Physiol. - London* **534**, 553 (2001).
- [49] M. Reconditi, *Rep. Prog. Phys.* **69**, 2709 (2006).
- [50] R. Sheshka and L. Truskinovsky, *Phys. Rev. E* **89**, 012708 (2014).
- [51] Z. Wu, R. L. Harne, and K. W. Wang, ASME 2014 Conference on Smart Materials, Adaptive Structures and Intelligent Systems, V002T06A019 (2014).
- [52] E. Eisenberg and T. Hill, *Prog. Biophys. Molec. Biol.* **33**, 55 (1978).
- [53] L. E. Ford, A. F. Huxley, and R. M. Simmons, *J. Physiol.* **269**, 441 (1977).
- [54] L. E. Ford, A. F. Huxley, and R. M. Simmons, *The Journal of physiology* **311**, 219 (1981).
- [55] H. Kojima, A. Ishiima, and T. Yanagida, *Proc. Natl. Acad. Sci. U.S.A.* **91**, 12962 (1994).
- [56] K. Wakabayashi, Y. Sugimoto, H. Tanake, Y. Ueno, Y. Takezawa, and Y. Amemiya, *Biophys. J.* **67**, 2422 (1994).
- [57] H. Huxley, A. Stewart, H. Sosa, and T. Irving, *Biophys. J.* **67**, 2411 (1994).
- [58] G. Piazzesi, M. Reconditi, M. Linari, L. Lucii, P. Bianco, E. Brunello, V. Decostre, A. Stewart, D. B. Gore, T. C. Irving, M. Irving, and V. Lombardi, *Cell* **131**, 784 (2007).
- [59] M. Irving, G. Piazzesi, L. Lucii, Y. Sun, J. Harford, I. Dobbie, M. Ferenczi, M. Reconditi, and V. Lombardi, *Nat. Struct. Biol.* **7**, 482 (2000).
- [60] A. V. Hill, *P Roy. Soc. Lond. B Bio.* **126**, 136 (1938).
- [61] G. Piazzesi, A. Reconditi, N. Koubassova, V. Decostre, M. Linari, L. Lucii, and V. Lombardi, *J. Physiol.* **549**, 93 (2003).
- [62] V. Decostre, P. Bianco, V. Lombardi, and G. Piazzesi, *Proc. Natl. Acad. Sci. USA* **102**, 13927 (2005).
- [63] K. W. Ranatunga, M. E. Coupland, G. J. Pinniger, H. Roots, and G. W. Offer, *J. Physiol.* **585**, 263 (2007).
- [64] M. Coupland and K. Ranatunga, *J. Physiol.* **548**, 439 (2003).
- [65] E. Homsher and C. J. Kean, *Annu. Rev. Physiol.* **40**, 93 (1978).
- [66] N. van Kampen, *Stochastic Processes in Physics and Chemistry* (North-Holland, Amsterdam, 2001).
- [67] Y. Suzuki and O. K. Dudko, *Phys. Rev. Lett.* **104**, 048101 (2010).
- [68] Y. V. Pereverzev, O. V. Prezhdo, M. Forero, E. V. Sokurenko, and W. E. Thomas, *Biophys. J.* **89**, 1446 (2005).
- [69] J.-D. Wen, M. Manosas, P. T. X. Li, S. B. Smith, C. Bustamante, F. Ritort, and I. Tinoco, *Biophys. J.* **92**, 2996 (2007).
- [70] D. T. Gillespie, *Journal of Computational Physics* **22**, 403 (1976).
- [71] T. Erdmann and U. S. Schwarz, *Phys. Rev. Lett.* **92**, 108102 (2004).